Encapsulation of Disodium-EDTA in Electrospun Polymeric Fibers for the Detection of Heavy Metals

Antonio Fotia, Patrizia Frontera, Lucio Bonaccorsi, Beniamino Sciacca, Angela Malara

▶ **To cite this version:**

Antonio Fotia, Patrizia Frontera, Lucio Bonaccorsi, Beniamino Sciacca, Angela Malara. Encapsulation of Disodium-EDTA in Electrospun Polymeric Fibers for the Detection of Heavy Metals. Advanced Sustainable Systems, 2023, 10.1002/adsu.202300463 . hal-04328036

HAL Id: hal-04328036
https://hal.science/hal-04328036

Submitted on 7 Dec 2023

HAL is a multi-disciplinary open access archive for the deposit and dissemination of scientific research documents, whether they are published or not. The documents may come from teaching and research institutions in France or abroad, or from public or private research centers.

L'archive ouverte pluridisciplinaire **HAL**, est destinée au dépôt et à la diffusion de documents scientifiques de niveau recherche, publiés ou non, émanant des établissements d'enseignement et de recherche français ou étrangers, des laboratoires publics ou privés.

Check for updates

ADVANCED SUSTAINABLE SYSTEMS
www.advsustainsys.com

Encapsulation of Disodium-EDTA in Electrospun Polymeric Fibers for the Detection of Heavy Metals

Antonio Fotia, Patrizia Frontera, Lucio Bonaccorsi, Beniamino Sciacca, and Angela Malara**

The contamination by heavy metals (HMs) is a pressing issue, due to their serious impact on the environment and human health. Therefore, the design and the development of a sensing material for their detection has gained a lot of attention. In this study, active layers are produced by the electrospinning technique, using three different polymers and disodium salt of ethylenediaminetetraacetic acid (Na_2-EDTA), known to be a chelating substance for heavy metals. The optimized active layer, in terms of polymer type, degree of encapsulation of the salt, as well as salt suitable content, is obtained and tested using the electrochemical impedance spectroscopy technique. The results of the sensing tests indicate the suitability of the developed electrospun layer for environmental monitoring. It is shown the detection of lead in the range of 10–100 000 µg L^{-1}, with a detection limit of 0.031 µg L^{-1}. Moreover, the system is proved to be robust against interfering contaminants such as thallium, another relevant heavy metal.

1. Introduction

In the last decades the significant industrial development and the consequent increasing urbanization, often related to many uncontrolled industrial discharges and unconscious waste management, have led to an exponential increase in the quantities of harmful substances released into the environment, especially dissolved in rivers, streams and aquifers.[1,2] In this context, contamination by heavy metals is becoming more than just an environmental issue rather a wider social problem due to the riskiness, toxicity and harmfulness of these substances that can accumulate in ecosystems, finally affecting human health, as outlined in the United Nation's Agenda 2030, goal 3 "Good health and Well-being." Despite trace concentrations of HMs in water do not pose serious dangers (note that some HM such as copper, selenium and zinc are essential to maintain the metabolism of the human body[3]), the monitoring of the threshold concentration and contextually the removal of the most harmful HMs, such as lead (Pb), mercury (Hg), cadmium (Cd), arsenic (As), chromium (Cr) and thallium (Tl), should be pursued. Many different methods have been explored in literature to determine the presence of HMs in solution, including atomic adsorption spectroscopy,[4] inductively coupled plasma optical emission spectrometry,[5] flameless atomic absorption spectrophotometry,[6] inductively coupled plasma mass spectrometry[7] and similar. However, although they are very selective and sensitive techniques, they require very expensive devices, with complex operating procedures and long measurement time. Electrochemical methods, unlike those previously mentioned, are affordable, user-friendly, involve simple procedures for the monitoring of contaminated samples and have a very short analysis time.[8–10] In addition, together with the monitoring of HM, their removal is also an important issue. In this regard, the use of chelating agents has been extensively treated[11] due to their ability to complex metals in a variety of industrial, domestic, and agricultural fields.[12–14] The most used is based on ethylenediaminetetraacetic acid (EDTA) and its salts, such as ethylenediaminetetraacetic acid disodium salt . This chelator shows a high selectivity to numerous HM ions in aqueous media, since it is possible to tailor it quite well by regulating the pH of the aqueous solution.[15] Therefore, since EDTA has favorable chelating and ion-exchange properties for many different metal ions, its immobilization on different supporting materials for metal adsorption purposes has received wide attention. Many examples of the use of EDTA to modify supports have been reported in the literature, and in all these cases EDTA was observed to form stable chelates with metals, suppressing their activities[16–23] and at

A. Fotia, P. Frontera, L. Bonaccorsi, A. Malara
Department of Civil
Energy
Environment and Material Engineering
Mediterranea University of Reggio Calabria
Reggio Calabria 89134, Italy
E-mail: antonio.fotia@unirc.it; angela.malara@unirc.it
B. Sciacca
Aix Marseille Univ
CNRS
CINaM
AMUtech
Marseille 13288, France

The ORCID identification number(s) for the author(s) of this article can be found under https://doi.org/10.1002/adsu.202300463

© 2023 The Authors. Advanced Sustainable Systems published by Wiley-VCH GmbH. This is an open access article under the terms of the Creative Commons Attribution License, which permits use, distribution and reproduction in any medium, provided the original work is properly cited.

DOI: 10.1002/adsu.202300463

the same time giving electrochemical signals for HMs quantification.

In particular, the dispersion of EDTA over a suitable support was considered of pivotal importance. For example, Dong et al. developed an ultra-sensitive electrochemical sensor able to detect lead, based on EDTA intercalated into layered double hydroxides (LDHs) supported on a carbon paste electrode.[17] A low-cost, rapid and sensitive electrochemical sensor based on an organic layer of EDTA-NQS (1,2-napthaquinone-4 sulphonic acid sodium salt) formed on the surface of a glassy carbon electrode was developed by Toghan et al.,[18] The results confirmed the complexation of the EDTA-NQS electrode surface with HM ions and showed a good activity, sensitivity, selectivity, stability, and reproducibility, with a very low detection limit for the simultaneous detection of different heavy metals, such as Cu^{2+}, Cd^{2+}, Hg^{2+}, Pb^{2+}, and Fe^{3+}.

In the study of Chen et al., EDTA was intercalated into LDHs by the coprecipitation method, and then encapsulated in a polymeric matrix of polyacrylonitrile (PAN) using the electrospinning technique. The performance of MgAl-EDTA-LDH@PAN electrospun nanofiber membrane was evaluated and proven for copper removal.[19] Deshmukh et al. proposed instead a nanocomposite material made by polypyrrole (Ppy) and single walled carbon nanotubes (SWNTs), that was successfully synthesized by an electrochemical method on a stainless-steel electrode. The functionalization with EDTA was performed using the dip coating technique at room temperature. The EDTA-Ppy/SWNTs modified stainless steel electrode exhibited good sensitivity and selectivity toward the detection of Pb(II) ions in aqueous media, showing a detection limit of 0.07 μM.[20]

Despite the numerous reported research and the complex solutions proposed, the crucial challenge lies in the conception and fabrication of an inexpensive and stable composite material able to halt the aqueous dissolution of embedded EDTA particles while maintaining their strong chelating properties. In this study, the evaluation of a simple and rapid method to disperse and durably confine the EDTA-based chelating agent in a suitable support is considered and discussed. In particular, it has been proposed its encapsulation in a polymeric fibrous structure obtained via the electrospinning technique, that is a consolidated and industrially-relevant procedure.[24–27] Electrospun nanofibers have indeed numerous advantageous characteristics, including a high surface-to-volume ratio, porous structures, and tunable properties (chemical composition, morphology, and dimensions).[28,29] Moreover, it was reported that the integration of nanomaterials as electrodes can improve the sensitivity and reproducibility of electrochemical methods[30] and the detection of HMs.[9]

This work introduces an upgraded use of Na_2-EDTA successfully and firmly encapsulated in an innovative layer made up of polymeric fibers. This enabled to achieve a stable and high activity of the salt in the detection and quantification of HMs in aqueous solutions. Specifically, the study was focused on the detection of Pb (II) ions, used as a model contaminant, to assess the performance of the functional material and demonstrate its proof of concept. The preparation procedure showed a good compromise between a fast and low-cost method and the production of high-quality and reliable materials for the development of sensitive layers.

2. Results and Discussions

Different polymer-based layers (polymethyl methacrylate, PMMA, polyvinyl acetate, PVAc and polystyrene, PS), with or without the addition of Na_2EDTA, were obtained through the electrospinning technique and characterized as summarized in **Table 1**. Among all the countless possibilities, specific criteria were followed in polymers selection. First, they were chose considering their availability, low cost and the opportunity for bioprocess derivation. Further featuring aspects, as three different backbone structures, functional properties and hydrophobicity,[31] were also considered, since resulting in different sensing performance. As reported, not all the salt concentrations yielded solutions suitable to be electrospun.[32]

Electrospun polystyrene system feature a morphology of rounded fibers with median diameter of 1.2 ± 0.2 μm, as shown in (**Figure 1**). The addition and further increase of Na_2EDTA content, promotes the change of morphology from rounded to flat. The increased solution viscosity, as a result of the salt content, can lead to a flattening or ribbon-like cross-section in the emerging fibers. The high viscosity can hinder the round cross-section typical of regular fibers, causing the fibers to take on a more flattened appearance,[1a] (see Figure S1, Supporting Information). Furthermore, the increasing of Na_2EDTA amount in the electrospun solution causes a slight increase of fibers diameter, achieving a value of 1.6 ± 0.2 μm for the highest concentration. It is worth noticing that Na_2EDTA particles resulted well encapsulated in the fibers for all the concentrations tested.

The morphology of electrospun PMMA systems results in rounded type fibers with median dimension of 0.9 ± 0.2 μm, as shown in **Figure 2**. The addition of Na_2EDTA salt seems not to significantly affect the morphology and the dimension of the fibers. Na_2EDTA particles resulted intercalated between fibers segments but not completely encapsulated.

The morphology of electrospun PVAc, reported in (**Figure 3**a), results in ribbon/flat fibers, probably due to the use of a high volatile solvent such as ethanol. The rapid vaporization of the solvent within the electrospinning jet leads to the formation of a skin layer, that collapses to form ribbons. However, the solvent volatility is not the only cause for the formation of ribbon-like fibers. Indeed, it is not just dependent on the polymer and solvent combination but also on the concentration of the solution. Koski et al.[33] reported flat ribbon fibers when the concentration of polyvinyl alcohol (PVA) was high or when higher molecular weights of PVA were used. Conversely, both lower concentration and lower molecular weight produced circular cross-section fibers. As shown in the zoomed image, some beads are also detected. According to Koombhongse et al.,[34] when the solvent escapes from the interior and, consequently the jet collapses, the skin on the beads collapses too, forming a toroid with a membrane that covers the hole. The addition of Na_2EDTA in the electrospun solution promotes the formation of the flat ribbon morphology, and the widening of fibers from ≈0,8 ± 0,2 μm to ≈2,0 ± 0,2 μm (Figure 3b). The increase of the salt content results in segregation and inhomogeneities, thus eluding the proposed purpose.

Moreover, as evidenced by high resolution SEM images for the highest possible salt concentration (1:1) (Figure S2, Supporting Information), it is interesting to highlight that, in accordance

© 2023 The Authors. Advanced Sustainable Systems published by Wiley-VCH GmbH

23667486, 0, Downloaded from https://onlinelibrary.wiley.com/doi/10.1002/adsu.202300463 by Cochrane France, Wiley Online Library on [06/12/2023]. See the Terms and Conditions (https://onlinelibrary.wiley.com/terms-and-conditions) on Wiley Online Library for rules of use; OA articles are governed by the applicable Creative Commons License

23667486, 0, Downloaded from https://onlinelibrary.wiley.com/doi/10.1002/adsu.202300463 by Cochrane France, Wiley Online Library on [06/12/2023]. See the Terms and Conditions (https://onlinelibrary.wiley.com/terms-and-conditions) on Wiley Online Library for rules of use; OA articles are governed by the applicable Creative Commons License

Table 1. Summary of the analyzed samples.

Sample name	Solvent	Weight ratio polymer/solvent	Weight ratio additive/polymer	Morphology obtained	Average diameter [μm]
PS	DMF*)	21.9/78.1	-	fibers	1.2 ± 0.2
PS-Na_2EDTA (1:0.1)	DMF	21.9/78.1	9.1/90.9	fibers	1.3 ± 0.2
PS-Na_2EDTA (1:0.25)	DMF	21.9/78.1	80.0/20.0	fibers	1.4 ± 0.2
PS-Na_2EDTA (1:1)	DMF	21.9/78.1	50.0/50.0	fibers	1.6 ± 0.2
PS-Na_2EDTA (1:2)	DMF	21.9/78.1	25.0/75.0	no suitable to be electrospun	
PMMA	DMF	7.5/92.5	-	fibers	0.9 ± 0.2
PMMA-Na2EDTA (1:0.1)	DMF	7.5/92.5	9.1/90.9	fibers	0.9 ± 0.2
PMMA-Na_2EDTA (1:0.25)	DMF	7.5/92.5	80.0/20.0	fibers	1.0 ± 0.2
PMMA-Na_2EDTA (1:1)	DMF	7.5/92.5	50.0/50.0	fibers	1.0 ± 0.2
PMMA-Na_2EDTA (1:2)	DMF	7.5/92.5	25.0/75.0	no suitable to be electrospun	
PVAc	EtOH (96%)**)	12.3/87.7	-	fibers	0.8 ± 0.2
PVAc-Na_2EDTA (1:0.1)	EtOH (96%)	12.3/87.7	9.1/90.9	fibers	2.0 ± 0.2
PVAc-Na_2EDTA (1:0.25)	EtOH (96%)	12.3/87.7	80.0/20.0	no suitable to be electrospun	
PVAc-Na_2EDTA (1:1)	EtOH (96%)	12.3/87.7	50.0/50.0	no suitable to be electrospun	
PVAc-Na_2EDTA (1:2)	EtOH (96%)	12.3/87.7	25.0/75.0	no suitable to be electrospun	

*) Dimethylformamide **) Ethanol

with EN ISO 527-2:2012 (Plastics – Determination of tensile properties – Part 2: Test conditions for moulding and extrusion plastics, ISO 527-2:2012), P-EDTA fibers are likely characterized by low thickness and high elasticity, since due to the deformation produced by particles encapsulation (15,3% of elongation), the texture of the surface is deformed in a sort of mesh-like structure. On the contrary, smooth and regular are fiber surfaces of PVAc-Na_2EDTA and PMMA-Na_2EDTA, both characterized by a higher thickness but a different deformation resistance (13,1% and 14,5% of elongation, respectively). Indeed, PVAc-Na_2EDTA sample gives evidence of fibers fractures nearby salt particles, that in turn result totally exposed; whereas, in the PMMA-Na_2EDTA sample a compact frame with entirely encapsulated particles is observed, due to both high thickness and elasticity of fibers. Different is the case of PS-Na_2EDTA system since the combination of low thickness and high elasticity results in a very thin and deformable polymer net able to complete cover salt particles but, at the same time, across which it is assured the interaction of the salt toward the surrounding environment, as also proved by pH test (see later).

EDX analysis fully agreed with the morphological characterization, further highlighting the different degree of encapsulation of salt particles in the polymeric fibrous matrix (**Figure 4**).

All recorder micro-Raman spectra showed the overlapping of the pristine polymers with the Na_2EDTA salt. Each spectrum is reported together with a spatial distribution map (see next). The Raman spectrum of polystyrene is more complex because the molecule is less symmetric and has hydrogen atoms in addition to carbon atoms. There are also different bond types connecting the atoms. The masses of the atoms involved and the strength of their bonds, affect the vibration's frequency. Low Raman shifts are found in heavy atoms and weak links. Strong bonds and light atoms have instead high Raman shifts. The polystyrene spectrum exhibits high frequency carbon-hydrogen (C—H) vibrations at a wavelength of roughly 3000 cm^{-1}. The low frequency carbon-carbon (C—C) vibration occur at ≈800 cm^{-1}. Because hydrogen is lighter than carbon, the C—H vibrations have a larger frequency than the C—C vibrations. The (C═C) double bond vibration appears at ≈1600 cm^{-1}, and the C—C at ≈800 cm^{-1} due to the weaker bond. Bond vibration rates are also influenced by the strength of the bond. As shown in the (**Figure 5**), the C—H vibration of polystyrene can be seen in two bands at about 2900 and 3050 cm^{-1}. The carbons in the former case are part of a carbon chains (referred to as "aliphatic"), whilst in the latter case are part of a carbon ring (referred to as "aromatic").

A complex molecule's vibration can be thought as being made up of numerous simple diatomic vibrations. However, it is only by taking into account the vibration of bigger groups of atoms that the entire complexity of the Raman spectrum can be fully appreciated (such as the aromatic carbon ring's expanding/constricting "breathing mode" that can be seen at 1000 cm^{-1} in polystyrene). Raman spectrum of PMMA (**Figure 6**) showed the characteristic band of PMMA at 2952 cm^{-1}. This band indicates C—H stretching and is the most prominent in the PMMA structure. The bands at 1645 cm^{-1} can be attributed to the combination band arising from n(C—C) and n(C—COO). The other Raman bands, such as those appearing at 604, 833, 995, 1264, 1470, 1739, and 3001 cm^{-1}, were in conformity with literature data.[35]

For the PVAc system the bands at 646, 921, 1428, 2112, and 2913 cm^{-1} were seen with large-intensity changes for each irradiation and they correspond to the modes of wagging of OH group (γw(OH)), stretching of C—C (ν(C—C)), bending of CH_2 and OH ($\delta(CH_2)$, δ(OH)), no assignment, stretching of CH of CH_2 group (ν(CH)), respectively (**Figure 7**).

© 2023 The Authors. Advanced Sustainable Systems published by Wiley-VCH GmbH

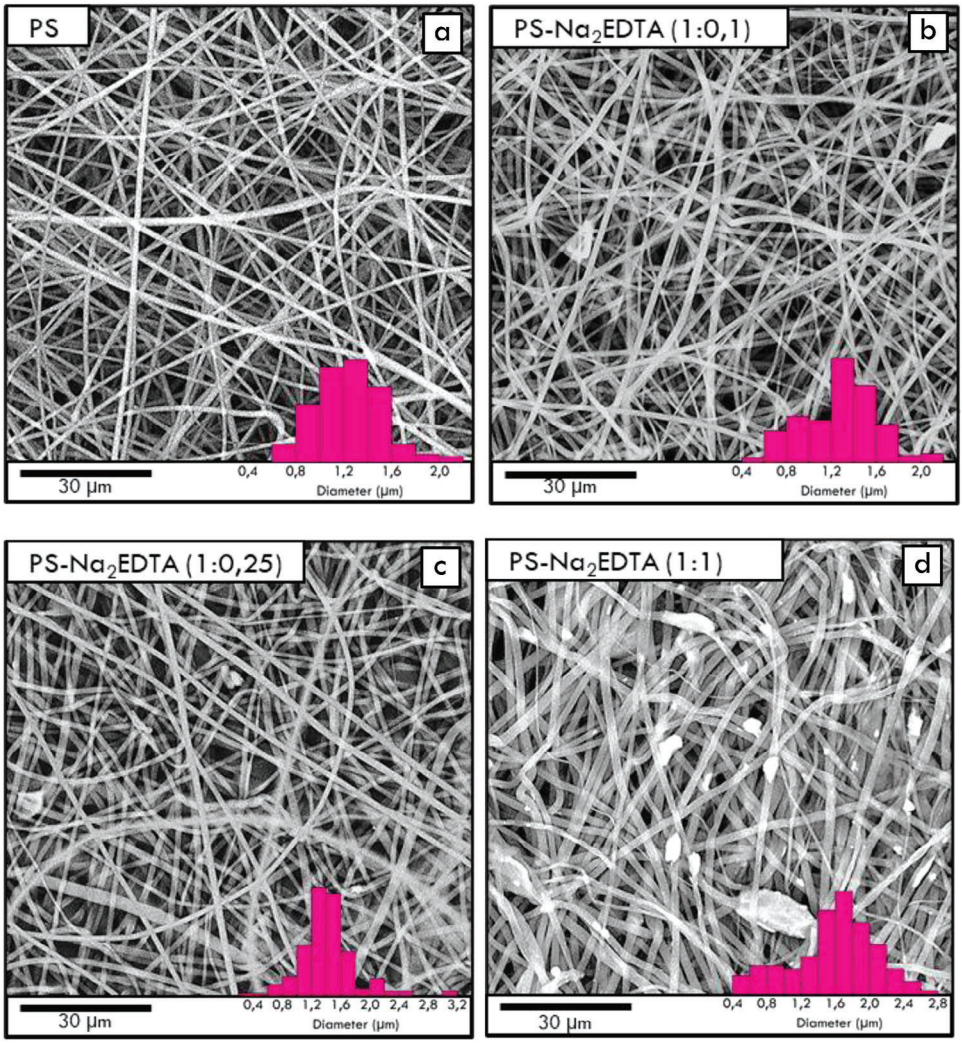

Figure 1. SEM images of a) PS, b) PS-Na_2EDTA(1:0.1), c) PS-Na_2EDTA(1:0.25), and d) PS-Na_2EDTA(1:1) samples.

Disodium ethylenediaminetetraacetate (Na_2EDTA) is a chelating agent containing carboxyl and amino groups, with a wide range of coordination properties. Through the Raman spectrum several infrared coherent bands can be distinguished. In the region from 2884 to 3021 cm^{-1}, the ν(C—H) stretch of the aliphatic CH_2 groups is detected. The small band at 3389 cm^{-1} corresponds to the deformation ν(O—H) of the water of hydration and another, at 1608 cm^{-1}, is caused by the angular deformation δ(H—O—H). It is worth mentioning that being a weak Raman scatterer, water related bands have low intensity.

The quantification of salt content into the fibrous layers was further confirmed by the weight loss carried out by the thermogravimetric analysis, as reported in detail in the supplementary information (Figures S3 and S4, Supporting Information). Briefly, the final residual mass, obtained for each sample, corresponds to the proportions of the salt used for the preparation of the polymeric solutions. Also, the X-ray diffraction analysis, confirms the loading of the salt in the polymeric layers (Figure S5, Supporting Information).

Samples were immersed in water (pH = 6) for up to 8 h to assess stability in highly stressed operational condition and determine any leaching of entrapped salt in aqueous solutions. The change of pH at room temperature (25 °C) was registered and analyzed as reported in **Figure 8**.

As term of comparison, the same quantity of salt entrapped inside the fibrous structure (13 mg) was solubilized in water (pH = 6), resulting in a pH decrease to 4.7. As evidenced, the equilibrium is reached within 15 min. When the composite fibers were tested instead, a different behavior was observed. In particular, the PS-Na_2EDTA system shows a narrow decrement of pH, suggesting that the salt is well entrapped in the layer. Differently, the PVAc-Na_2EDTA exhibits a significant pH decrease, indicating the solubilization of the salt, that leaches from the polymeric layer. Conversely, the PMMA polymer encapsulates the Na_2EDTA salt entirely, as inferred from the unvaried pH, proved the complete confinement of salt particles inside fibers, unable to interact with the surrounding environment.

Owing to the featuring structure, as well as to the optimized configuration, PS-Na_2EDTA (1:1) sample (for brevity named

© 2023 The Authors. Advanced Sustainable Systems published by Wiley-VCH GmbH

23667486, 0, Downloaded from https://onlinelibrary.wiley.com/doi/10.1002/adsu.202300463 by Cochrane France, Wiley Online Library on [06/12/2023]. See the Terms and Conditions (https://onlinelibrary.wiley.com/terms-and-conditions) on Wiley Online Library for rules of use; OA articles are governed by the applicable Creative Commons License

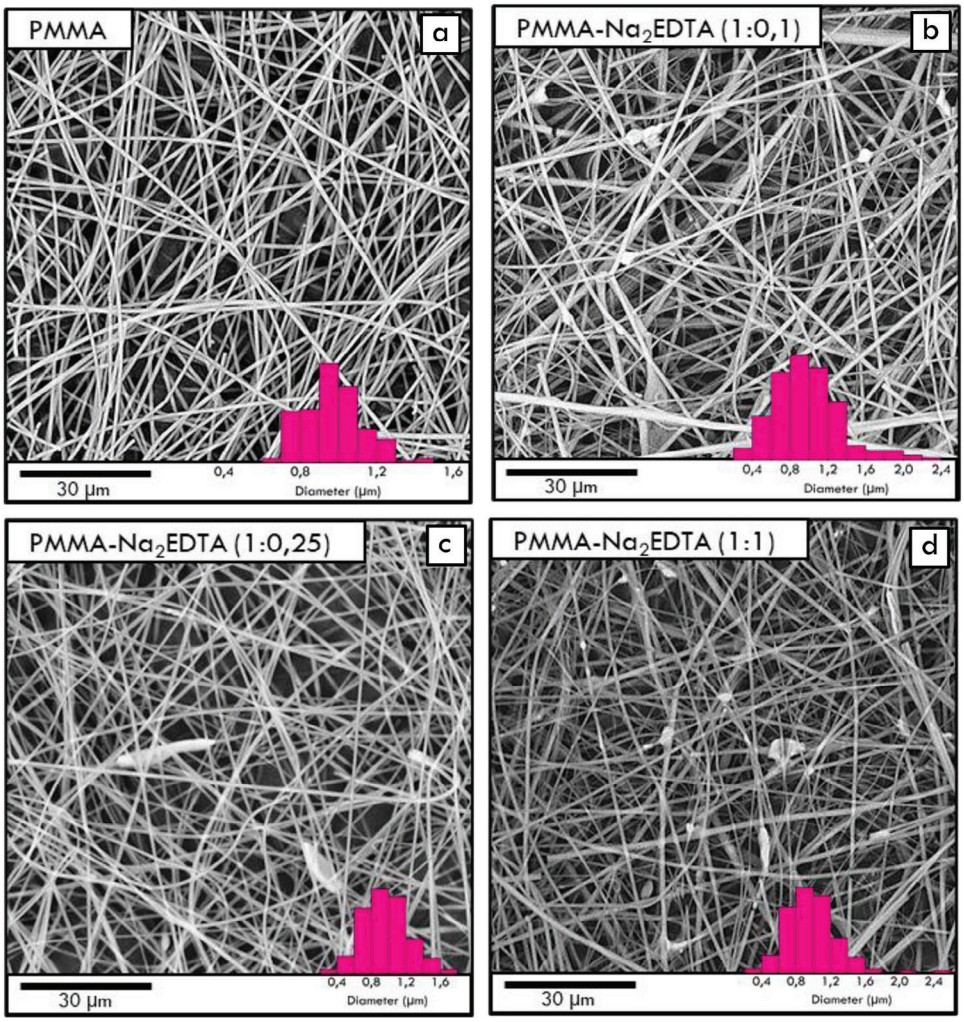

Figure 2. SEM images of a) PMMA, b) PMMA-Na_2EDTA(1:0.1), c) PMMA-Na_2EDTA(1:0.25), and d) PMMA-Na_2EDTA(1:1) samples.

PS-EDTA in the following), characterized by the highest content of Na_2EDTA salt, was finally used as the active layer for the implementation of the sensing device.

EIS curves are reported for both PS and PS-EDTA sensors, using the Nyquist plot (**Figure 9**). Each point on the Nyquist plot is an impedance value at a frequency point. In the X-axis, impedance at the right side of the plot is registered at low frequency, while, at higher frequencies, the generated impedances are read on the left.

As evidenced by results, impedance values in doped sample (PS-EDTA) were lower than in the case of pure PS for all the tested concentrations of Pb, indicating that Na_2EDTA has a

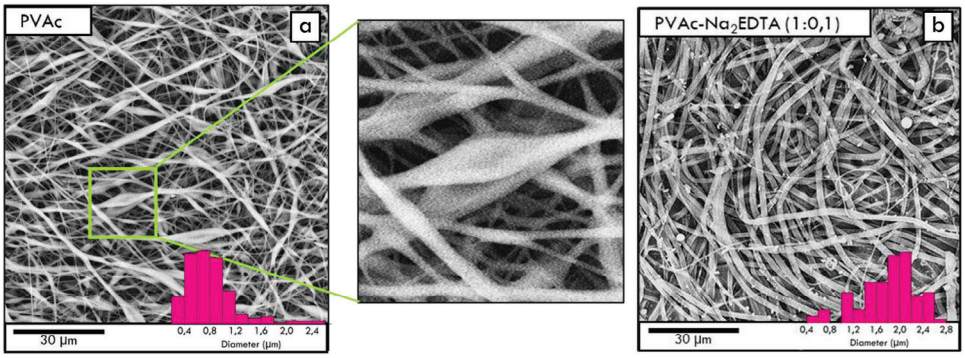

Figure 3. SEM images of a) PVAc sample and its detailed fibers; b) PVAc-Na_2EDTA (1:0.1) sample.

© 2023 The Authors. Advanced Sustainable Systems published by Wiley-VCH GmbH

23667486, 0, Downloaded from https://onlinelibrary.wiley.com/doi/10.1002/adsu.202300463 by Cochrane France, Wiley Online Library on [06/12/2023]. See the Terms and Conditions (https://onlinelibrary.wiley.com/terms-and-conditions) on Wiley Online Library for rules of use; OA articles are governed by the applicable Creative Commons License

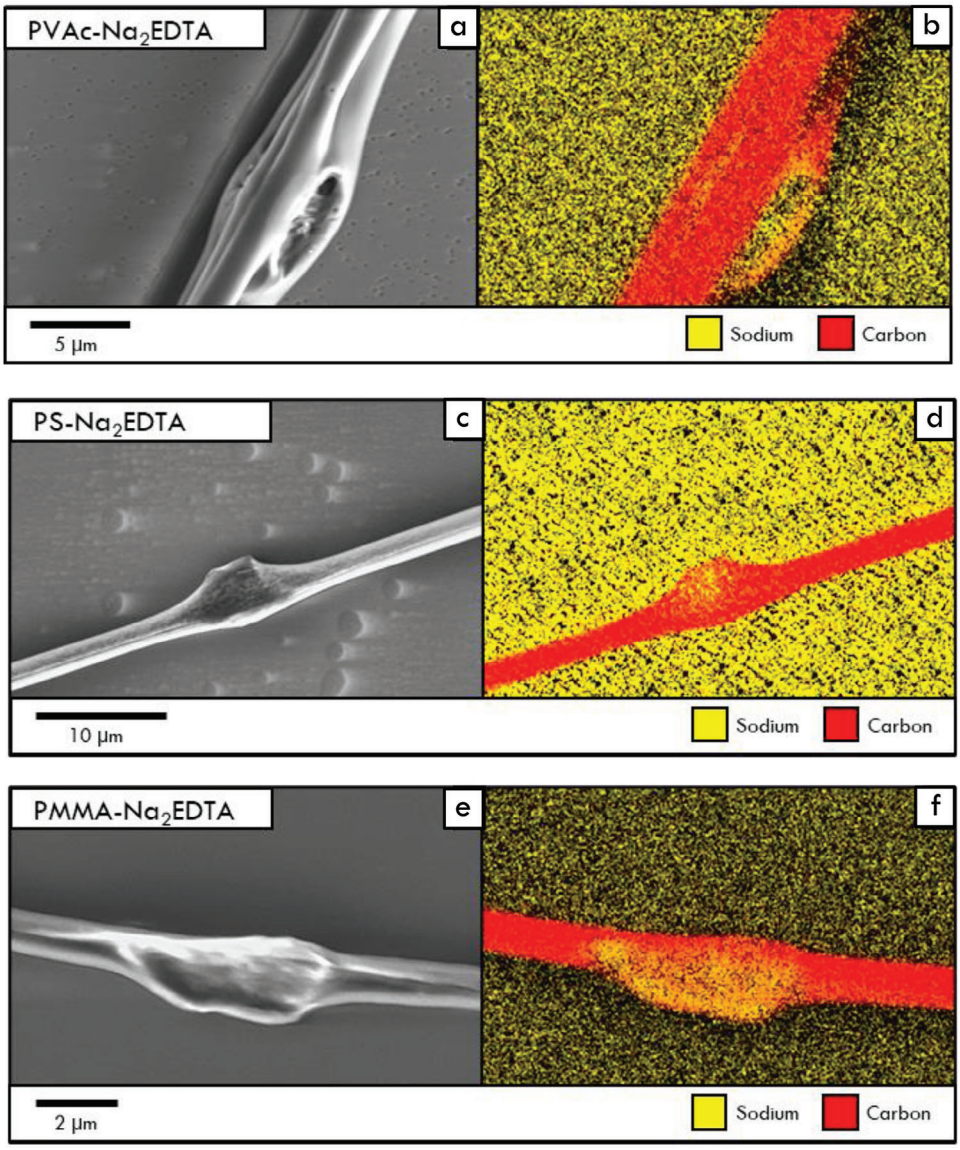

Figure 4. Detailed SEM-EDX analysis of samples: a,b) PVAc, c,d) PS, and e,f) PMMA with Na_2EDTA additive in 1:1 ratio.

strong influence on the sample conductivity. This is consistent with previous literature reporting that Na_2EDTA dissolved in aqueous solution can work as an electron donor, promoting the accumulation of electrons in the conduction band.[36]

It should be also considered that the electrochemical reactions that occur at the metal/film and film^{-1} solution interfaces of the barrier layer contribute to the impedance of a system. Since the total impedance of the system comprises all the contributions of the interfacial phenomena, including those at the metal/film^{-1} solution interphase and the resistance of the solution, electrical circuits are often used to analyze experimental results.[37]

More detailed interpretation can be obtained by impedance curve modelling. In particular, it is well known that in the Nyquist diagram an arc represents a process, whose electrical nature is simultaneously resistive (charge conduction mechanism) and capacitive (polarization or charges separation mechanism), with an associated time constant ($t = R_C$). To this purpose a simplified Randles circuit was used for PS-EDTA sample whereas a CPE (Constant Phase Elements) model was adopted for the pure PS sample, characterized by a straight line in the Nyquist plot.

From the equivalent electrical model (**Figure 10**), the values of the electrical components are obtained using the least-squares minimization fitting of the electrochemical impedance spectroscopy spectrum. The variables that are involved in this technique are the resistance solution (Rs), the charge transfer resistance (Rct), and double layer capacitance (CPE)[38] whose values are reported in (**Table 2**).

PS curves were approximated to straight lines over a frequency range of 2500 Hz–1 MHz. The fitted Rct was very large in this case, and the corresponding circuit was simplified by a CPE.[39] In this case the ion transport was hindered due

© 2023 The Authors. Advanced Sustainable Systems published by Wiley-VCH GmbH

23667486, 0, Downloaded from https://onlinelibrary.wiley.com/doi/10.1002/adsu.202300463 by Cochrane France, Wiley Online Library on [06/12/2023]. See the Terms and Conditions (https://onlinelibrary.wiley.com/terms-and-conditions) on Wiley Online Library for rules of use; OA articles are governed by the applicable Creative Commons License

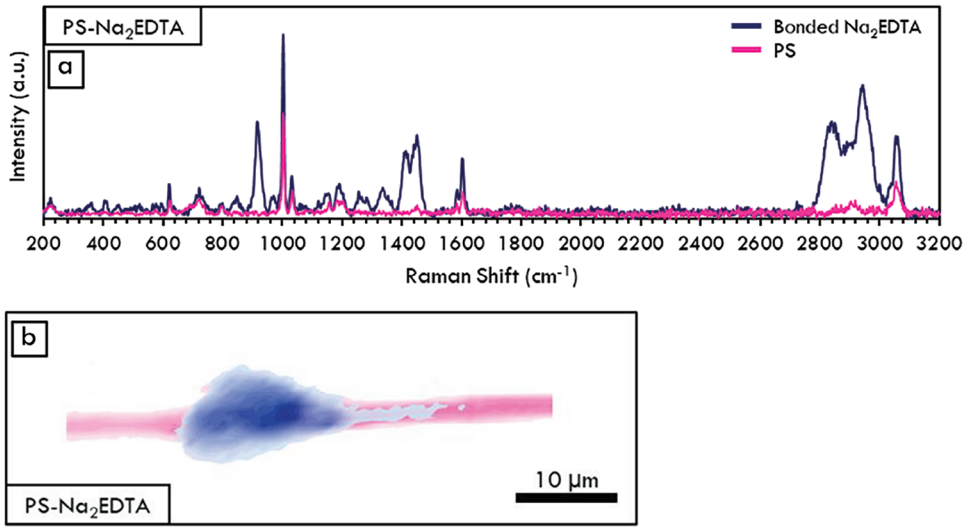

Figure 5. a) Raman spectra of PS and PS-Na_2EDTA samples; b) Raman map of PS-Na_2EDTA sample. The blue color is used for the Na_2EDTA encapsulated in the PS fiber and the fuchsia color is used for the pure PS fiber.

to a discontinuous coverage of Pb on the film surface in the absence of the chelating agent. Only a bare adsorption of Pb ions (proportional to its concentration in the solution) could be observed, as suggested by the slight increase of the impedance values.

The characteristic semicircle arc, related to the parallel combination of a resistor and a capacitor in the case of PS-EDTA sample, indicates the presence of ionic charge carriers due to the presence of the chelating agent. Moreover, the significant deformation of the impedance semicircles, flattened with respect to the ideal case, is caused by the higher Rct values, that increase with increasing Pb concentration. The value of Rct is associated with electron transfer reactions such as electron-hole recombination. An equilibrium in the salt dissociation ($EDTA^{-2}/Na^{+2}$) was reached when PS-Na_2EDTA sensor active layer was conditioned in the buffer solutions, indicating that Na_2EDTA was well encapsulated in the structure of porous PS fibers. In this condition a distribution of negative charges on the surface of the active layer/solution barrier is formed and $EDTA^{-2}$ is able to bind Pb^{+2} ions. The complex obtained is stable and proportional to the content of lead ions. Indeed, increasing the contaminant concentration, the Rct increased hindering the reduction of EDTA negative charges and the consequent formation of stable PS-Pb/EDTA complexes on the surface of the active layer, as depicted in the scheme of (**Figure 11**).

In **Figure 12** it is presented the impact of Pb(II) ions concentration on Rct, showing a linear behavior at low concentration.

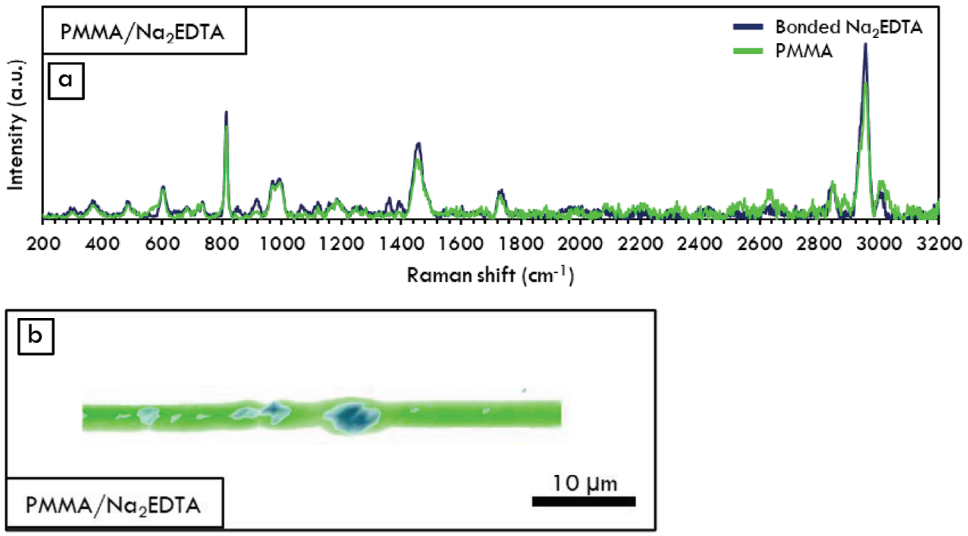

Figure 6. a) Raman spectra of PMMA and PMMA-Na_2EDTA samples; b) Raman map of PMMA-Na_2EDTA sample. The blue color is used for the Na_2EDTA encapsulated in the PMMA fiber and the green color is used for the pure PMMA fiber.

© 2023 The Authors. Advanced Sustainable Systems published by Wiley-VCH GmbH

23667486, 0, Downloaded from https://onlinelibrary.wiley.com/doi/10.1002/adsu.202300463 by Cochrane France, Wiley Online Library on [06/12/2023]. See the Terms and Conditions (https://onlinelibrary.wiley.com/terms-and-conditions) on Wiley Online Library for rules of use; OA articles are governed by the applicable Creative Commons License

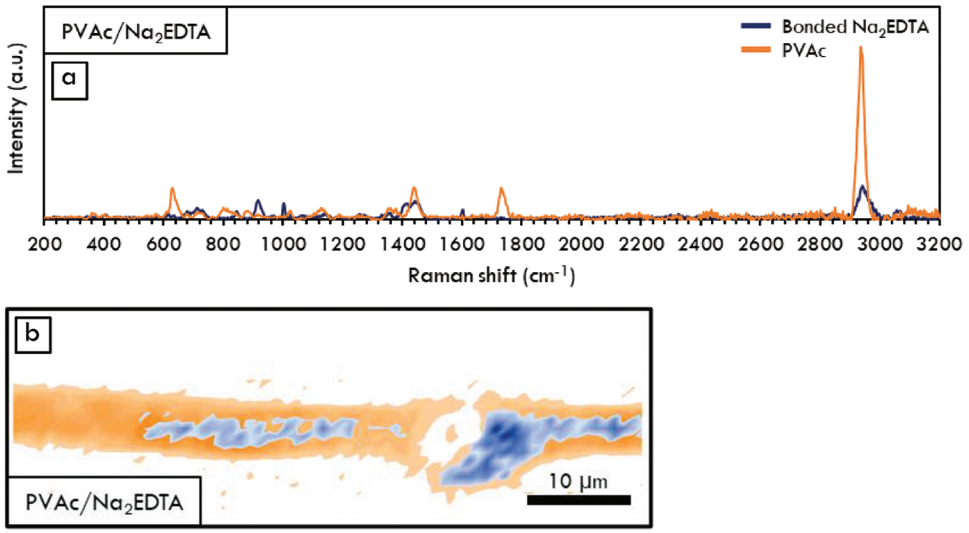

Figure 7. a) Raman spectra of PVAc and PVAc-Na_2EDTA samples; b) Raman map of PVAc-Na_2EDTA sample. The blue color is used for the Na_2EDTA encapsulated in the PVAc fiber and the orange color is used for the pure PMMA fiber.

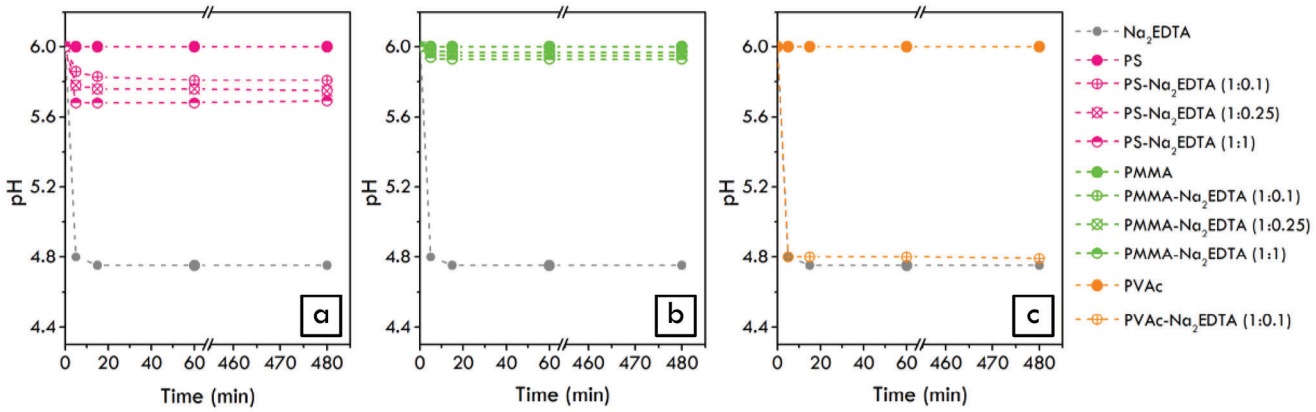

Figure 8. Trend of pH for the different analyzed systems a) PS-Na_2EDTA b) PMMA-Na_2EDTA c) PVAc-Na_2EDTA compared to pure Na_2EDTA salt.

Table 2. Values relative of PtIDE*)-PS and PtIDE*)-PSNa_2EDTA.

Solution	Rs [Ohm]	Q [F*s^(n−1)]	n	Rct [Ohm]
		PtIDE-PS		
Blank	100.1 ± 2.61	1.86e-6 ± 0.56e-7	0.898 ± 0.025	-
10 µg L^{-1} Pb	96.52 ± 2.92	1.69e-6 ± 0.49e-7	0.930 ± 0.028	-
100 µg L^{-1} Pb	97.06 ± 2.73	1.64e-6 ± 0.41e-7	0.931 ± 0.031	-
1 mg L^{-1} Pb	93.75 ± 2.75	1.25e-6 ± 0.35e-7	0.924 ± 0.024	-
100 mg L^{-1} Pb	91.44 ± 2.69	1.25e-6 ± 0.39e-7	0.930 ± 0.025	-
		PtIDE-PSNa_2EDTA		
Blank	44.3 ± 1.21	4.90e-6 ± 0.15e-6	0.878 ± 0.026	0.285e6 ± 0.855e4
10 µg L^{-1} Pb	44.3 ± 1.26	4.70e-6 ± 0.16e-6	0.882 ± 0.031	0.366e6 ± 1.09e4
100 µg L^{-1} Pb	44.9 ± 1.35	4.67e-6 ± 0.13e-6	0.880 ± 0.029	0.376e6 ± 1.12e4
1 mg L^{-1} Pb	45.09 ± 1.44	4.68e-6 ± 0.11e-6	0.881 ± 0.028	0.479e6 ± 1.29e4
100 mg L^{-1} Pb	45.15 ± 1.56	4.75e-6 ± 0.17e-6	0.880 ± 0.031	1.056e6 ± 3.17e4

*) Platinum Interdigitated Electrodes

© 2023 The Authors. Advanced Sustainable Systems published by Wiley-VCH GmbH

23667486, 0, Downloaded from https://onlinelibrary.wiley.com/doi/10.1002/adsu.202300463 by Cochrane France, Wiley Online Library on [06/12/2023]. See the Terms and Conditions (https://onlinelibrary.wiley.com/terms-and-conditions) on Wiley Online Library for rules of use; OA articles are governed by the applicable Creative Commons License

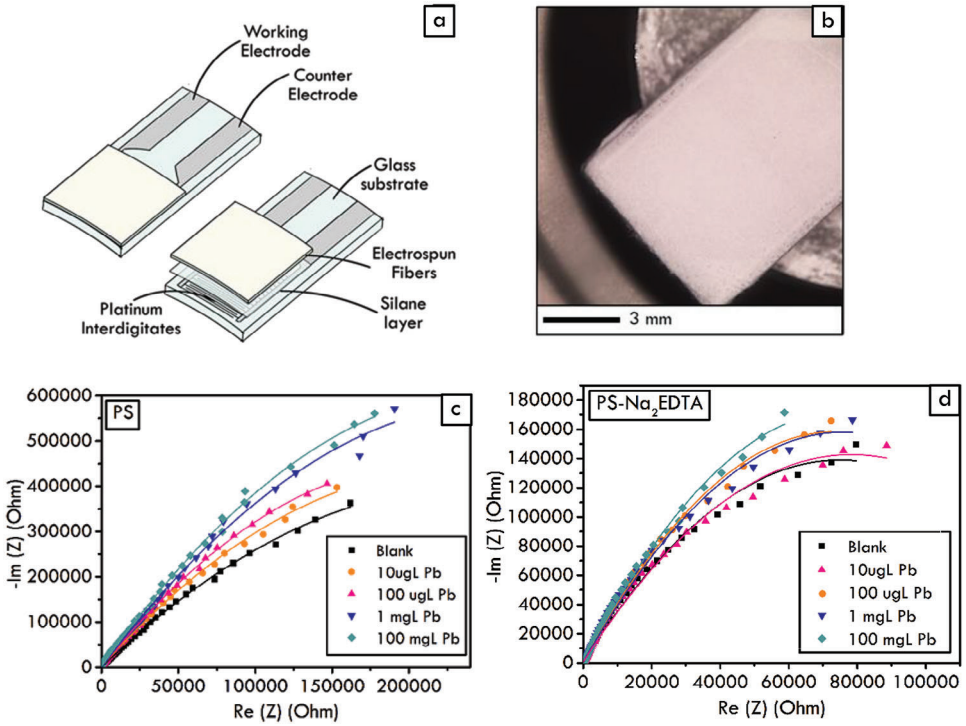

Figure 9. a) Schematic representation of active layers electrospun over supports, b) zoomed image of PS-EDTA sensor, and impedance curves registered for c) PS and d) PS-Na_2EDTA samples at increasing Pb(II) concentration.

The limit of detection (LOD) for Pb(II) ions was calculated using the following formula[40]:

$$\text{LOD} = 3.3 \times \frac{\text{standard deviation of the regression line } (\sigma)}{\text{Slope (S)}} \quad (1)$$

The calculated value of the limit of detection for Pb(II) was 0.031 μg L^{-1}.

The variation of Rct values of PS-EDTA sample, normalized with respect to the Rct_0 value registered in the blank solution, is reported in **Figure 13**. .

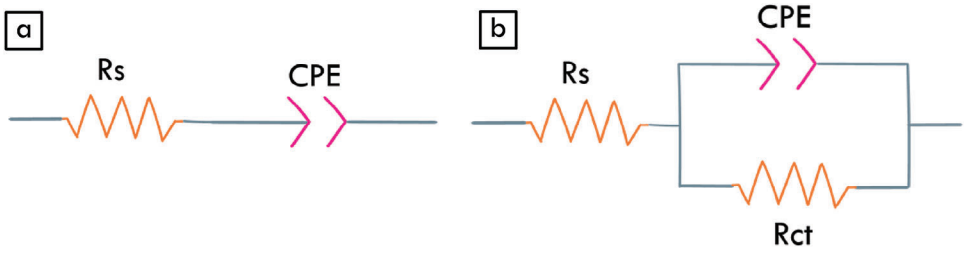

Figure 10. a) Resistance solution in series with CPE, b) Simplified Randles circuit.

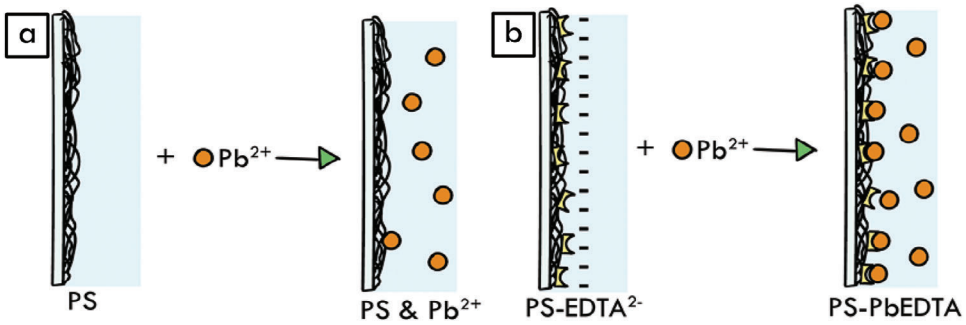

Figure 11. Schematic representation of the interaction between the surface of the active layer and Pb ions.

© 2023 The Authors. Advanced Sustainable Systems published by Wiley-VCH GmbH

23667486, 0, Downloaded from https://onlinelibrary.wiley.com/doi/10.1002/adsu.202300463 by Cochrane France, Wiley Online Library on [06/12/2023]. See the Terms and Conditions (https://onlinelibrary.wiley.com/terms-and-conditions) on Wiley Online Library for rules of use; OA articles are governed by the applicable Creative Commons License

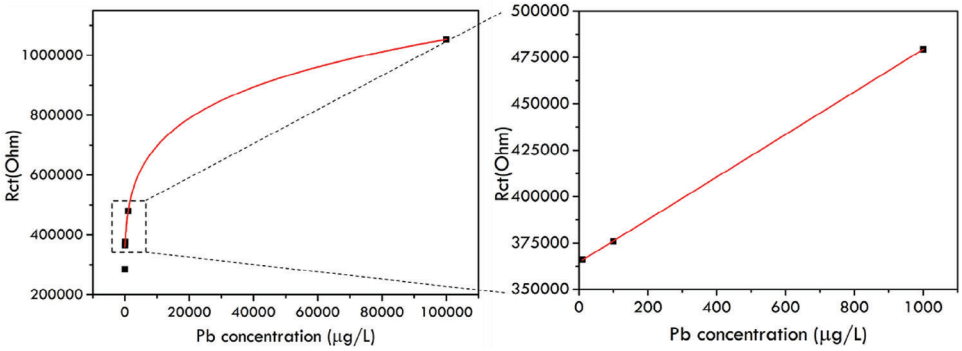

Figure 12. Rct values plotted against Pb (II) concentrations with a detail at Pb low concentrations.

It is important to highlight that the reported measurements were recorded at a fixed pH value of the buffer solution, equal to 4.5 and suitable to favor the interaction mechanism between $EDTA^{-2}$ and Pb^{+2}. Both the adsorbent, as well as the pH, can impact the Pb adsorption process, via cation exchange, complexation, and precipitation.[41]

Specifically, in the case of lead in aqueous systems, the initial pH influences both the states of the functional groups on the surface of the adsorbent and the existing form of the metal ions in solution. In aqueous solution with pH ranging between 2.0 and 8.0, it is known that lead species can exist in three forms: Pb^{2+}, $Pb(OH)^{+}$ and $Pb(OH)_2$.[16] For a pH value lower than 6.0, the dominant species is Pb^{2+}, the hydrolysis of Pb^{2+} to form $Pb(OH)^{+}$ and $Pb(OH)_2$ starts at pH 3.7 and 6.8, respectively. Finally, over pH > 7.5, the dominant species becomes $Pb(OH)^{+}$.[16] The strong pH dependent adsorption suggested that the adsorption of Pb (II) was dominated by ion exchange and surface complexation. Under acidic conditions, the functional groups of dissociated EDTA were negatively charged, showing an electrostatic attraction to Pb^{2+} and finding it easy to donate their electron pairs to coordinate with Pb^{2+}. This provides first Pb adsorption and then Pb-EDTA complexation, enhancing Pb immobilization onto the EDTA.

Finally, considering that EDTA shows a high selectivity to numerous heavy metal ions by regulating the pH of the solution,[15] it was evaluated the formation of EDTA complexes with other heavy metal species as a function of pH. Based on the equilibrium constants, thallium (Tl^{+}) was chosen as a model interfering species. Thallium is an extremely toxic heavy metal even if at low concentration, posing substantial risks to ecosystem and human health. As well as lead it is widely discharged from industries in wastewaters. Therefore, the performance of the PS-EDTA sensor was tested through EIS measurements in the same operational conditions as described in the case of lead, at a pH value of 4.5 but using Tl^{+} as an interfering contaminant. By increasing the thallium concentration, the impedance did not vary significantly (see Figure 13), showing no response to interfering species. This suggests the high ability of the sensor to detect a specific heavy metal when the pH value is precisely regulated.

3. Conclusion

The design and development of an active layer for the detection of heavy metals in aqueous solution was hypothesized, discussed and tested.

Potential active layers were obtained through the electrospinning technique, using three different polymers and disodium salt of EDTA, known to be a chelating substance for heavy metals.

Despite the possibility to obtain self-standing layers with the considered polymers, some differences occurred in the immobilization/encapsulation of salt. Then, among all the tested systems, polystyrene was chosen for its good capability to maintain entrapped Na_2EDTA grains, due to its surface features. The optimized active layer, in terms of Na_2EDTA concentration (additive/polymer weight ratio = 50.0/50.0), was implemented in an

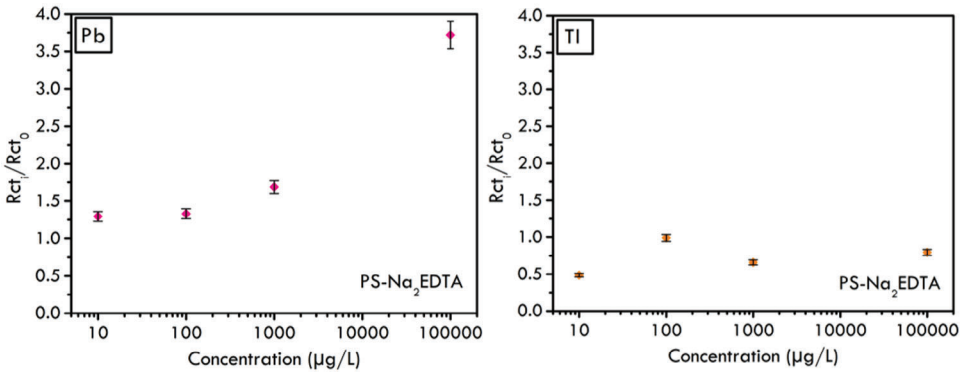

Figure 13. Normalized Rct values detected in the case of increasing Pb and Tl concentrations.

© 2023 The Authors. Advanced Sustainable Systems published by Wiley-VCH GmbH

23667486, 0, Downloaded from https://onlinelibrary.wiley.com/doi/10.1002/adsu.202300463 by Cochrane France, Wiley Online Library on [06/12/2023]. See the Terms and Conditions (https://onlinelibrary.wiley.com/terms-and-conditions) on Wiley Online Library for rules of use; OA articles are governed by the applicable Creative Commons License

Table 3. Summary of electrospun samples, used solvents and electrospinning parameters.

Sample name	Solvent	Weight ratio polymer/solvent	Weight ratio additive/polymer	Speed and time stirring	Voltage [KV]	Flow rate [mL h^{-1}]	NCD [cm]
PS	DMF	21.9/78.1	-	600 rpm- 4h	12.5	0.900	15.0
PS-Na_2EDTA (1:0.1)	DMF	21.9/78.1	9.1/90.9	600 rpm- 4h	11.5	0.900	15.0
PS-Na_2EDTA (1:0.25)	DMF	21.9/78.1	20.0/80.0	600 rpm- 4h	11.0	0.900	15.0
PS-Na_2EDTA (1:1)	DMF	21.9/78.1	50.0/50.0	600 rpm- 4h	10.5	0.900	15.0
PS-Na_2EDTA (1:2)	DMF	21.9/78.1	75.0/25.0	600 rpm- 4h	no suitable to be electrospun		
PMMA	DMF	7.5/92.5	-	600 rpm- 4h	12.5	0.600	13.0
PMMA-Na_2EDTA (1:0.1)	DMF	7.5/92.5	9.1/90.9	600 rpm- 4h	11.5	0.600	13.0
PMMA-Na_2EDTA (1:0.25)	DMF	7.5/92.5	20.0/80.0	600 rpm- 4h	11.5	0.600	13.0
PMMA-Na_2EDTA (1:1)	DMF	7.5/92.5	50.0/50.0	600 rpm- 4h	11.0	0.600	13.0
PMMA-Na_2EDTA (1:2)	DMF	7.5/92.5	75.0/25.0	600 rpm- 4h	no suitable to be electrospun		
PVAc	EtOH (96%)	12.3/87.7	-	500 rpm- 3h	13.0	0.800	13.0
PVAc-Na_2EDTA (1:0.1)	EtOH (96%)	12.3/87.7	9.1/90.9	500 rpm- 3h	11.5	0.800	13.0
PVAc-Na_2EDTA (1:0.25)	EtOH (96%)	12.3/87.7	20.0/80.0	500 rpm- 3h	no suitable to be electrospun		
PVAc-Na_2EDTA (1:1)	EtOH (96%)	12.3/87.7	50.0/50.0	500 rpm- 3h	no suitable to be electrospun		
PVAc-Na_2EDTA (1:2)	EtOH (96%)	12.3/87.7	75.0/25.0	500 rpm- 3h	no suitable to be electrospun		

impedimetric PtIDE-PS-Na_2EDTA sensor, by the direct collection of fibers over its surface.

The sensing tests of the active layer were carried out using the electrochemical impedance spectroscopy technique at different concentrations of lead and thallium, used as an interfering contaminant. The results of the sensing tests showed that the sensor with PS/Na_2EDTA active layer was able to detect different Pb concentrations in the range 10–100 000 µg L^{-1}. Moreover, according to the pH value of the solution, the high sensibility toward lead with respect to other heavy metals, as thallium, was demonstrated.

The proposed active layer finally resulted a cheap and simple solution for a potential application in the environmental monitoring.

4. Experimental Section

Materials: Poly(methyl methacrylate) (PMMA) (average Mw = 996 000), poly(vinyl acetate) (PVAc) (average Mw = 500 000), poly(styrene) (PS) (average Mw = 192 000), ethanol (96% purity), ethylenediaminetetraacetic acid disodium salt dihydrate (Na_2EDTA), dimethylformamide (DMF), trimethoxy(propyl)silane (97%) were used for the production of fibers. Sodium acetate, glacial acetic acid (≥99.7%), lead nitrate and thallium nitrate were used to prepare the pollutant solutions. All reagents were purchased from Sigma Aldrich, USA and used without any further purification.

Synthesis of Active Layer: In order to produce the optimal active layer for the heavy metal detection, several sensing materials were produced, using three different polymers, PMMA, PVAc, and PS, with or without the addition of Na_2EDTA, in numerous experimental conditions. Typically, the polymer is dissolved in its solvent to produce the electrospinnable solution, whereas, in the preparation of polymeric solutions with the addition of the disodium salt of EDTA (Na_2EDTA), a further step is required. First, the additive is dispersed in the solvent using an ultrasonic bath, the mixture is stirred for 2 min and finally the polymer is added. All the prepared solutions were stirred at room temperature, at different speed rate, depending on the solution type. Several tests, as detailed in (**Table 3**), were carried out in order to optimize the active layer parameters .

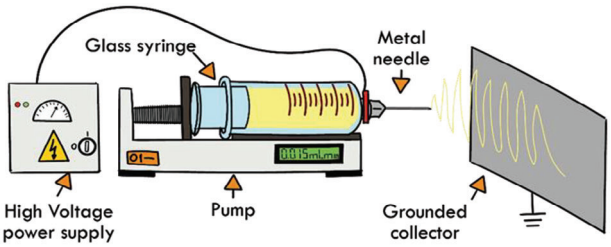

Figure 14. Electrospinning setup.

For the electrospinning process, polymeric solutions were loaded into a 10 mL glass syringe connected to a 0.7 mm metal needle. A pump was used to control the flow rate, while different applied voltage and needle-to-collector distance (NCD) were tested (**Figure 14**). The electrospinning process was performed at 25 °C with a relative humidity of 30%. The (Table 3) provides a summary of the electrospinning parameters used for each sample.

Fibers were directly collected over the sensing substrate, fixed on aluminum foils and connected to the ground. In detail, two interdigitates (Pt-IDEs), the working electrode (WE) and the counter electrode (CE), made of platinum on a glass substrate from Metrohm DropSens (Herisau, Switzerland), were used for the realization of the sensing device. The dimensions of the glass substrate were 22.8 mm in length, 7.6 mm in width, and 0.7 mm in thickness. Each of the interdigitated electrodes had 125 digits with a bands/gaps equal to 5 µm. In order to increase the adhesion with the fibers, each Pt-IDEs's surface was spin-coated with a 200 ± 20 µm silane solution.

Samples were characterized by complementary investigation techniques.

A Phenom Pro-X scanning electron microscope equipped with an energy-dispersive X-ray spectrometer was utilized for the preliminary characterization of electrospun materials. A detailed investigation was performed through a high-resolution scanning electron microscope, Jeol JSM-7900F, specialized in low accelerating voltages studies and low vacuum measurements. The system was coupled with a chemical microanalysis system using X-ray spectrometry (BRUKER Esprit).

© 2023 The Authors. Advanced Sustainable Systems published by Wiley-VCH GmbH

23667486, 0, Downloaded from https://onlinelibrary.wiley.com/doi/10.1002/adsu.202300463 by Cochrane France, Wiley Online Library on [06/12/2023]. See the Terms and Conditions (https://onlinelibrary.wiley.com/terms-and-conditions) on Wiley Online Library for rules of use; OA articles are governed by the applicable Creative Commons License

Materials crystalline structure was investigated using a Bruker D2 Phaser with CuKα radiation at 30 kV and 20 mA. Peaks attribution was made according with COD (Crystallographic Open Database). The diffraction angles 2θ were varied between 10° and 80° in steps of 0.02° and a count time of 5 s per step.

Thermogravimetric TGA/DSC analysis was performed with a Netzsch instrument. The temperature-programmed experiments were carried out in the range 25–1000 °C, under a total air flow rate of 100 cc min^{-1} with a heating rate of 5 °C min^{-1}.

Raman Spectroscopy was performed on a Renishaw system connected to a microscope with a motorized stage that allows for mapping. A He-Ne laser with a 633 nm wavelength was used as the excitation source. A 100× objective (NA 0.85) was used to excite and collect scattered light. Spectra were collected in the range of 200–3200 cm^{-1}. Each spectrum was reported together with a spatial distribution map, generated using for each system the peak area intensity in specific regions as reported in the following: 790.8– 829.7 cm^{-1} for PMMA and 879.2–933.9 cm^{-1} for Na_2EDTA in PMMA/ Na_2EDTA system; 985.9–1044.3 cm^{-1} for PS and 880.8–982.8 cm^{-1} for Na_2EDTA in PS/ Na_2EDTA system; 881.2–983.2 cm^{-1} for PVAc and 599.4–670.9 cm^{-1} for Na_2EDTA in PVAc/ Na_2EDTA system.

EIS measurements were carried out using an AMEL 7050 galvanostat/potentiostat coupled with an AMEL 7200 frequency response analyzer with a three-electrode configuration. A platinum wire with a diameter of 0.5 mm and a length of 100 mm was used as a reference electrode. As a buffer solution, 0.012 M stock was prepared using concentrated acetic acid (CH_3COOH) and sodium acetate (CH_3COONa). This 4.5 pH solution was obtained using equimolar mixtures of acetic acid and sodium acetate. The concentrations were respectively 10 µg L^{-1}, 100 µg L^{-1}, 1 mg L^{-1}, and 100 mg L^{-1} for each contaminant examined. The volume of solution used for each measurement was 3 mL and the electrochemical cell was shielded with a Faraday cage. The EIS measurements were performed with a half-wave amplitude of 10 mVpK and a frequency range of 0.1 to 100.000 Hz. No potential bias was applied. Ten measurement cycles were performed for each concentration, with a 45-s interval between each. All measurement cycles for each concentration of the single contaminant were conducted using the same electrodes.

Supporting Information

Supporting Information is available from the Wiley Online Library or from the author.

Conflict of Interest

The authors declare no conflict of interest.

Data Availability Statement

The data that support the findings of this study are available from the corresponding author upon reasonable request.

Keywords

disodium-EDTA, electrochemical sensors, electrospinning, heavy metals, hybrid fibers

Received: September 26, 2023
Revised: November 21, 2023
Published online:

[1] a) M. K. Singh, A. Singh, *Characterization of Polymers and Fibers*, Woodhead Publishing, Sawston, **2021**. b) A. Neeraj, R. Y. Hiranmai, K. Iqbal, *Land Degrad. Dev.* **2023**, *34*, 173.
[2] H. Yao, J. Lu, X. Yuan, J. Wu, J. Zhao, X. Yu, Y. Zhou, *CLEAN–Soil, Air, Water* **2014**, *42*, 331.
[3] A. Malara, E. Paone, P. Frontera, L. Bonaccorsi, G. Panzera, F. Mauriello, *Sustainability* **2018**, *10*, 3547.
[4] K. Siraj, S. A. Kitte, *Int. J. Chem. Anal. Sci.* **2013**, *4*, 201.
[5] A. M. Massadeh, A. A. Alomary, S. Mir, F. A. Momani, H. I. Haddad, Y. A. Hadad, *Environ. Sci. Pollut. Res.* **2016**, *23*, 13424.
[6] A. R. Ipeaiyeda, A. R. Ayoade, *Appl. Water. Sci.* **2017**, *7*, 4449.
[7] J. Q. Mccomb, C. Rogers, F. X. Han, P. B. Tchounwou, *Water Air Soil Pollut.* **2014**, *225*, 2169.
[8] L. A. Malik, A. Bashir, A. Qureashi, A. H. Pandith, *Environ. Chem. Lett.* **2019**, *17*, 1495.
[9] A. Malara, A. Fotia, E. Paone, G. Serrano, *Materials* **2021**, *14*, 3000.
[10] E. L. Sciuto, S. Petralia, J. R. Van Der Meer, S. Conoci, *Biotechnol. Bioeng.* **2021**, *118*, 1456.
[11] B. Nowack, J. M. VanBriesen, *Chelating Agents in the Environment*, ACS Publications, Washington DC **2005**.
[12] T. A. Saleh, M. Mustaqeem, M. Khaled, *Environ. Nanotechnol. Monit. Manag.* **2022**, *17*, 100617.
[13] S. Gluhar, A. Kaurin, D. Lestan, *Chemosphere* **2020**, *257*, 127226.
[14] R. Li, Q. Li, X. Sun, J. Li, J. Shen, W. Han, L. Wang, *J. Colloid Interface Sci.* **2019**, *542*, 379.
[15] J. McMurry, *Organic Chemistry*, 6th Ed, Thomson-Brooks/Cole, Belmont **2004**.
[16] J. Huang, M. Ye, Y. Qu, L. Chu, R. Chen, Q. He, D. Xu, *J. Colloid Interface Sci.* **2012**, *385*, 137.
[17] J. Dong, Q. Fang, H. He, Y. Zhang, J. Xu, Y. Sun, *Microchim. Acta* **2015**, *182*, 653.
[18] A. Toghan, M. Abd-Elsabour, A. M. Abo-Bakr, *Sens. Actuators, A* **2021**, *322*, 112603.
[19] H. Chen, J. Lin, N. Zhang, L. Chen, S. Zhong, Y. Wang, W. Zhang, Q. Ling, *J. Hazard. Mater.* **2018**, *345*, 1.
[20] M. A. Deshmukh, G. A. Bodkhe, S. Shirsat, A. Ramanavicius, M. D. Shirsat, *Front. Chem.* **2018**, *6*, 451.
[21] M. Singh, D. Vaya, R. Kumar, B. Das, *J. Serb. Chem. Soc.* **2021**, *86*, 327.
[22] S. Meena, D. Vaya, B. K. Das, *Bull. Mater. Sci.* **2016**, *39*, 1735.
[23] M. Verma, W. Ahmad, J.-H. Park, V. Kumar, M. S. Vlaskin, D. Vaya, H. Kim, *J. Water Process Eng.* **2022**, *49*, 102989.
[24] B. G. Seethu, S. P. Aditya, P. Devikrishna, H. Kulkarni, M. E. Emerald, C. Grover, H. A. Pushpadass, *Mater. Sci. Engin. Food Prod. Dev.* **2023**. https://doi.org/10.1002/9781119860594.ch14
[25] A. Malara, P. Frontera, L. Bonaccorsi, P. Antonucci, *Materials* **2018**, *11*, 2555.
[26] L. Bonaccorsi, A. Fotia, A. Malara, P. Frontera, *Energies (Basel)* **2020**, *13*, 4299.
[27] A. Freni, L. Calabrese, A. Malara, P. Frontera, L. Bonaccorsi, *Energy* **2019**, *187*, 115971.
[28] Y. Huang, Y. Miao, T. Liu, *J. Appl. Polym. Sci.* **2014**, *131*, 5829.
[29] A. Fotia, A. Malara, E. Paone, L. Bonaccorsi, P. Frontera, G. Serrano, A. Caneschi, *Nanomaterials* **2021**, *11*, 1269.
[30] A. Malara, S. G. Leonardi, A. Bonavita, E. Fazio, S. Stelitano, G. Neri, F. Neri, S. Santangelo, *Mater. Chem. Phys.* **2016**, *184*, 269.
[31] J. C. Foster, I. Akar, M. C. Grocott, A. K. Pearce, R. T. Mathers, R. K. O'reilly, *ACS Macro Lett.* **2020**, *9*, 1700.
[32] X.-H. Qin, E.-L. Yang, N. Li, S.-Y. Wang, *J. Appl. Polym. Sci.* **2007**, *103*, 3865.
[33] A. Koski, K. Yim, S. Shivkumar, *Mater. Lett.* **2004**, *58*, 493.

© 2023 The Authors. Advanced Sustainable Systems published by Wiley-VCH GmbH

23667486, 0, Downloaded from https://onlinelibrary.wiley.com/doi/10.1002/adsu.202300463 by Cochrane France, Wiley Online Library on [06/12/2023]. See the Terms and Conditions (https://onlinelibrary.wiley.com/terms-and-conditions) on Wiley Online Library for rules of use; OA articles are governed by the applicable Creative Commons License

[34] S. Koombhongse, W. Liu, D. H. Reneker, *J. Polym. Sci., Part B* **2001**, *39*, 2598.
[35] K. J. Thomas, M. Sheeba, V. P. N. Nampoori, C. P. G. Vallabhan, P. Radhakrishnan, *J. Opt. A: Pure Appl. Opt.* **2008**, *10*, 055303.
[36] K. Maeda, *Adv. Mater.* **2019**, *31*, 1808205.
[37] S. Wang, J. Zhang, O. Gharbi, V. Vivier, M. Gao, M. E. Orazem, *Nat. Rev. Methods Primers* **2021**, *1*, 41.
[38] B. Petovar, K. Xhanari, M. Finsgar, *Anal. Chim. Acta* **2018**, *1004*, 10.
[39] D. Zhang, J. Tong, B. Xia, Q. Xue, *Sens. Actuators, B* **2014**, *203*, 263.
[40] M. A. Deshmukh, H. K. Patil, G. A. Bodkhe, M. Yasuzawa, P. Koinkar, A. Ramanaviciene, M. D. Shirsat, A. Ramanavicius, *Sens. Actuators, B* **2018**, *260*, 331.
[41] H. Li, X. Dong, E. B. Da Silva, L. M. De Oliveira, Y. Chen, L. Q. Ma, *Chemosphere* **2017**, *178*, 466.

© 2023 The Authors. Advanced Sustainable Systems published by Wiley-VCH GmbH

23667486, 0, Downloaded from https://onlinelibrary.wiley.com/doi/10.1002/adsu.202300463 by Cochrane France, Wiley Online Library on [06/12/2023]. See the Terms and Conditions (https://onlinelibrary.wiley.com/terms-and-conditions) on Wiley Online Library for rules of use; OA articles are governed by the applicable Creative Commons License